Benchmarking Three-Dimensional Thermal Model against Field Measurement on the Thermal Response of an Insulating Concrete Form (ICF) Wall in Cold Climate

Hamed H. Saber, PhD

Wahid Maref, PhD
Member ASHRAE

Marianne Armstrong

Michael C. Swinton, PE
Member ASHRAE

Madeleine Z. Rousseau

Ganapathy Gnanamurugan

ABSTRACT

Field monitoring of the dynamic heat transmission characteristics through Insulating Concrete Form (ICF) wall assemblies was undertaken in 2009–2010 at National Research Council Canada's Institute for Research in Construction's (NRC-IRC) Field Exposure of Walls Facility (FEWF). The main objective of this research is to evaluate the dynamic heat transmission characteristics through two mid-scale ICF wall assemblies in FEWF for a one-year cycle of exposure to outdoor natural weathering conditions. The scope of work included the design of the experiments, installation of test specimens, commissioning of the instrumentation, operation of the test facility, monitoring, and data collection & analysis. The present NRC-IRC's hygrothermal model, called hygIRC-C, was used to interpret the readings of the instrumentations and to improve the experiment design by repositioning these instrumentations at critical locations. Subsequently, the present model was benchmarked against the measured data. Results showed that the predictions of the present model are in good agreement with experimental data. This research is on-going. Future work will be presented in later publications where the present model will be used to conduct numerical simulations in order to investigate the transient thermal response of full-scale ICF wall assemblies subjected to different Canadian climates.

INTRODUCTION AND BACKGROUND

Increasingly, home builders are turning toward a variety of construction methods to improve thermal performance while reducing the cost of construction. While Insulating Concrete Form (ICF) technology dates back to the late 1960s in Europe, ICF construction has only caught on in North America for use in residential and commercial construction over the last two decades (Hersh Servo AG 2010). Generally modern ICFs consist of stackable formwork made of expanded polystyrene foam, which is filled on site with concrete, and then remains in place to provide permanent insulation. ICF technology offers the potential to improve air tightness and energy performance over the current practice of wood frame construction. With the growing presence of ICF construction in the market, it is important to gain an understanding of their actual performance in the field, and the role played by the thermal mass of the concrete in regulating heat losses.

A number of research projects have been performed on the thermal performance and thermal mass to investigate the potential of annual energy saving compared to traditional light-weight construction. The benefit of thermal mass was extensively investigated, especially at the Oak Ridge National Laboratory (Burch et al. 1984a; Burch et al. 1984b; Burch et al. 1984c; Christian 1991; Kosny et al. 1998; Kosny et al. 2001; Christian et al. 1998; Kossecka and Kosny 1998). Petrie et al. (2001) conducted field investigation of two side-by-side houses in Knoxville, Tennessee. The two houses were similar except one house had Insulating Concrete Form (ICF) exterior walls and the other house had conventional wood-framed exterior walls. The results showed that the ICF house used 7.5% less energy than the conventional house. This work has shown that the principal benefit of thermal mass on thermal performance is to dampen fluctuations in interior conditions during significant fluctuations in outdoor conditions. Additionally, Petrie et al. (2001) conducted numerical simulations using

Hamed H. Saber *is a research officer,* ***Wahid Maref*** *is a senior research officer,* ***Marianne Armstrong*** *is a resarch council officer,* ***Michael C. Swinton*** *is a principal research officer, and* ***Ganapathy Gnanamurugan*** *is a technical officer with the National Research Council Canada, Institute for Research in Construction, Ottawa, Ontario, Canada.* ***Madeleine Z. Rousseau*** *is retired from her role as a research council officer with the National Research Council Canada, Institute for Research in Construction.*

DOE2 software to investigate the effect of different climates of six U.S. cities (Phoenix, Minneapolis, Dallas, Boulder, Knoxville, and Miami) on the energy consumption of both the ICF and conventional wood-framed houses. The results of cooling, heating, and total electricity usage showed that the thermal mass had benefits for both cooling and heating. The ICF houses used 5.5% to 8.5% less energy annually than the conventional wood-framed houses. This range of saving (5.5% to 8.5%) agreed with Kosny's prediction of 4% to 10% savings with ICF houses compared to conventional wood-framed houses for 10 U.S. climates (Kosny et al. 2001).

In 1999, NAHB Research Centre tested three side-by-side homes with floor area of 102 m^2 (1098 ft^2) to compare the energy performance of two ICF homes (one had an ICF plank system and one had an ICF block system) versus a conventional wood-framed home (2×4 wall stud framing, sheathed with OSB, and insulated with fiberglass batt in the wall cavities) (NAHB 1999). The three homes were located on the same street in Chestertown, Maryland. Also, the three homes had identical orientation, window area, roof construction, footprint, ductwork, and air handler systems. The testing was conducted over a one-year period beginning in April 1998. Heating consumption composed of two periods, April 1, 1998 through June 1, 1998 and October 6, 1998 through March 16, 1999. Cooling consumption represented the period from June 1, 1998 through September 22, 1998. This study showed that a 20% difference was noticed between ICF houses and the conventional wood-frame house's energy consumption. This difference can be attributed primarily to the higher effective R-value of the ICF walls and continuous insulation at the slab. The insulation for the walls of the ICF homes is R-20 while the wall insulation of the wood-framed home is R-13. The solid wall surfaces for all three homes make up approximately 44% of the total surface area of the homes (the remainder being made up of the ceiling area, windows, and doors). A 50% increase in the solid wall surface area resistance to conductive heat loss (R-20 compared to R-13) represented significant increased energy-efficiency. The foundation/slab details showed the impact clearly on the wood-frame home and demonstrated greater heat loss in February and greater heat gain in August as evidenced by the wood-frame home's more pronounced and direct response to outdoor temperature changes. Given the total area and the thermal conductivity of materials involved, the foundation/insulation/slab detail of the wood-frame home represented a significant source of heat loss and gain not evidenced in the ICF homes.

In 2001, the Portland Cement Association conducted a modeling study of the energy use of single-family houses with various exterior walls using DOE 2.1 software (Gajda 2001). This study presented two ICF options: (1) concrete sandwiched by two insulation layers, and (2) insulation sandwiched by two concrete layers. The study examined the performance of eleven different types of exterior walls in 25 North American locations to determine the expected differences in energy use. In this study, the only differences for a given location were the exterior wall type and the capacity of the HVAC system. The results showed that houses with concrete walls had lower heating and cooling costs than walls with light construction, and contributed to additional savings through a reduction in the required heating and cooling system capacity.

In 2006, a project was conducted by Enermodal Engineering Limited for Canada Mortgage and Housing Corporation (CMHC) and the Ready Mix Concrete Associate of Ontario (RMCAO) to study the performance of a seven-story insulating concrete form multi-residential building in Waterloo, Canada (Hill and Monsour 2006). Temperatures through the wall assembly were monitored at eight locations from December 1, 2005 to February 26, 2006. The project reported little contribution of the concrete to the steady-state R-value. During transient conditions, heat storage effects were reported. While the concrete never supplied heat to the interior during the winter monitoring period, the measured data showed that concrete did temper heat loss to the exterior during the periods of cold weather.

Recently, the National Research Council of Canada's Institute for Research in Construction (NRC-IRC) in collaboration with Canada Mortgage and Housing Corporation (CMHC) and Natural Resources Canada (NRCan) proposed evaluating the thermal response of two ICF wall assemblies in NRC-I RC's Field Exposure of Walls Facility (FEWF) for a one-year cycle of exposure to outdoor natural weathering conditions. The FEWF allows field monitoring of the thermal response of side-by-side test wall specimens exposed to natural weathering on the exterior and exposed to controlled indoor conditions.

This paper presents information generated from this project in order to understand and quantify the effect of thermal mass of the concrete in the ICF wall systems in Canadian cold climate. The objective of this paper is to use the present NRC-IRC' hygrothermal model called "hygIRC-C" used to interpret the readings of the instrumentations and to improve the experiment design by selecting the appropriate locations of instrumentation. Next, the present model is benchmarked by comparing its prediction against the test results. After gaining confidence in the simulation tool, it will be used to investigate the effect of the thermal mass of the concrete and EPS on the thermal response of the ICF assembly subjected to different Canadian climate conditions.

The hygIRC-C model uses COMSOL Multiphysics (COMSOL) as a solver. This model solves simultaneously the highly nonlinear two-dimensional and three-dimensional Heat, Air, and Moisture (HAM) equations. These equations were discretized using the Finite Element Method (FEM). This model has been used in several related studies (Elmahdy et al. 2009; Saber et al. 2010a, 2010b; Saber and Swinton 2010). The three-dimensional version of this model was used to conduct numerical simulations for different full-scale wall assemblies with and without penetration to represent window in order to predict the effective thermal resistance (R-value)

with and without air leakage. These walls incorporated two different types of insulation, specifically, spray polyurethane foam and glass fiber. The predicted R-values for these walls were in good agreement (within + 5%) with the measured R-values in NRC-IRC's Guarded Hot Box (GHB) (Elmahdy et al. 2009; Saber et al. 2010a). Recently, the two-dimensional version of the present model was used to conduct numerical simulations in order to investigate the effect of the emissivity of foil on the effective thermal resistance of a foundation wall system with foil bonded to expanded polystyrene foam in a furred assembly with airspace next to the foil (Saber and Swinton 2010). In this work (Elmahdy et al. 2009; Saber et al. 2010a; Saber and Swinton 2010), no moisture transport was accounted for in predicting the thermal performance of different types of walls.

In the case of accounting for moisture transport, the present model was used to predict the drying rate of a number of wall assemblies subjected to different exterior and interior boundary conditions (Saber et al. 2010b). The results showed that the overall agreements between the present model and the hygIRC-2D model that was previously developed and benchmarked at NRC-IRC (Maref et al. 2002) as well as the experimental measurements were good in terms of the shapes of the drying and drying rate curves. Additionally, the predicted average moisture content of the different wall assemblies over the test periods were in good agreement, all being within +5% of those measured. Another step for benchmarking the present model is to compare its predictions against field measurements as opposed to controlled lab of the thermal response of mid-scale ICF walls. As indicated earlier, these walls are being tested and subjected to different exterior and interior conditions. The descriptions of the wall specimens and experimental approach are briefly discussed in the next sections.

ICF WALL ASSEMBLIES AND INSTRUMENTATION

Two ICF wall test specimens were installed side-by-side in the FEWF. The dimensions of the test specimens are shown in Figure 1. For repeatability purposes, the two test specimens were identical in order to provide an indication of the variability of results under similar exposure conditions. Prior to preparing the two ICF specimens, the present model was used to determine the thickness of the thermal insulation needed around and between the ICF specimens to minimize the thermal interaction between the specimens and the rest of the FEWF walls. The ICF wall is comprised of an external layer of expanded polystyrene foam, EPS (nominal thickness of 2.5 in.), a layer of concrete (6 in. thick) and an interior layer of EPS (2.5 in. thick). The ICF has plastic spanners to connect the layers of EPS and reinforced with horizontal and vertical steel bars prior to pouring the concrete. The specimens were allowed to cure outdoors for 28 days before being lifted into place by forklift on August 25, 2009. The ICF test specimens were covered with a painted drywall on the interior. The exterior of the ICFs was covered by a vinyl siding that is resistant to rainwater ingress, as rain water ingress and its effects on heat transmission characteristics are not intended to be included in the study.

In each wall specimen, four heat flux transducers were installed at the center of the wall as shown in Figure 1 at the following interfaces: (1) between the vinyl siding and the exterior EPS foam layer, (2) on the face of the concrete behind the exterior EPS foam layer, (3) on the face of the concrete behind the interior EPS foam layer, and (4) between the drywall and the interior EPS foam layer. At each of these interfaces, two thermocouples were installed at each of the five instrumentation locations shown in Figure 1, for a total of 10 thermocouples per interface. As a part of the test protocol, all heat flux transducers used in the two ICF test specimens were calibrated according to the ASTM C 1130-07 "Standard Practice for Calibrating Thin Heat Flux Transducers"(2009). The uncertainly of heat flux measurements was ±5%. Also, the uncertainty of thermocouples measurements was ±0.1°C. More details about the test protocol and results will be presented in later publications.

GENERAL PARAMETERS AFFECTING THE THERMAL RESPONSE OF WALL SYSTEMS

The thermal properties of the concrete layer of the ICF wall assembly are listed in Table 1 (Hill and Monsour 2006). Recently, the thermal conductivity and density of the type of EPS layer that was used in the ICF wall were measured at the NRC-IRC's material characterization laboratory at different temperatures. The test method used to measure the thermal conductivity of EPS was ASTM C 518-04 (2007). The measured thermal conductivity of EPS, λ_{eff} (in W/(mK)), as a function of temperature, T (in °C), that was used in the numerical simulation is given as:

$$\lambda_{eff} = 1.062\times10^{-4}T + 0.0308 \quad (1)$$

The uncertainty of the measured thermal conductivity of EPS was +1.5%. The measured density of EPS was 22.7 kg/m^3 (uncertainty = +0.6 kg/m^3). Also, the thermal properties of glass fiber with a thickness of 140 mm that can fill the stud cavities of a 2 in. × 6 in. wood frame construction are listed in Table 1 as a reference just for a purpose of explaining the effect of material properties on the transient response of wall systems.

There are four main parameters that affect the thermal response of a wall system. These parameters are:

1. Volumetric heat capacity, sometimes called thermal mass. This is a measure of the ability of the material to store thermal energy. In the case of the ICF wall, the concrete has the ability to store energy of 75 times that for EPS. Furthermore, the ICF wall has the ability to store thermal energy of ~ 200 times that for glass fiber.
2. Thermal diffusivity, $\alpha = \lambda_{eff}/(\rho Cp)$. This is the ability of the material to conduct thermal energy relative to its ability to store thermal energy. The material with low

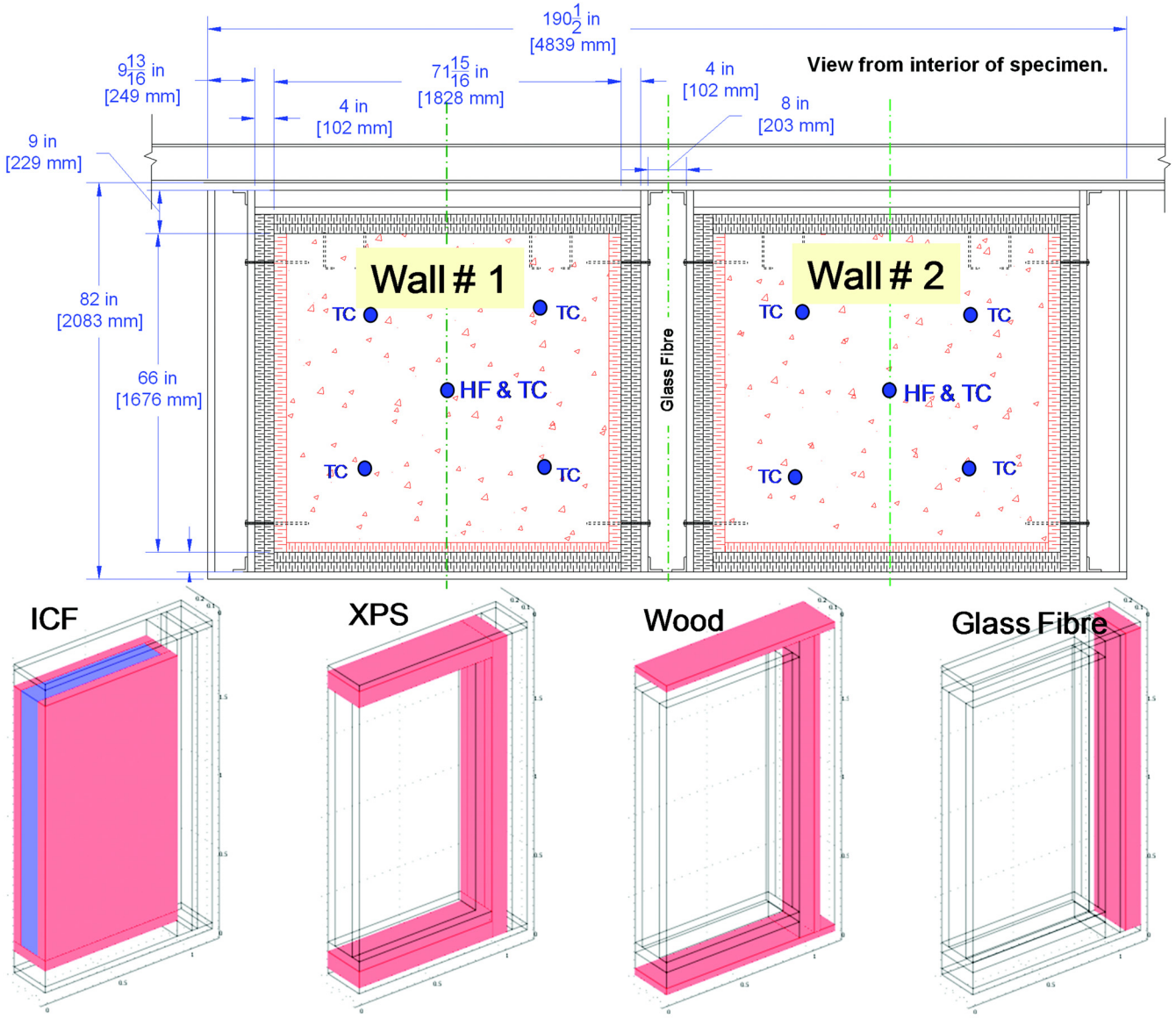

Figure 1 *Schematic of ICF wall specimens showing the instrumentation (heat flux transducers, HF, and thermocouples, TC) and three-dimensional representation of half of ICF wall.*

thermal diffusivity responds slower to changes in the thermal environment compared to that with high thermal diffusivity. As shown in Table 1, the EPS and glass fibre respond to the thermal changes 3 times and 6 times, respectively, faster than the concrete.

3. Thermal resistance (R-value). It is a measure of the material ability to resist the heat flow. As shown in Table 1, both the ICF components and the glass fiber in reference wall have approximately the same R-value (R-20). Unlike the ICF wall, the reference wall with glass fiber has thermal bridges through the wood/steel studs. In a recent study at NRC-IRC (Elmahdy et al. 2009 and Saber et al. 2010a), the measured R-value in the NRC-IRC' Guarded Hot Box (GHB) for a full-scale glass fiber wall assembly (2.4 m × 2.4 m) and 2 in. × 6 in. wood studs at 16 in. o/c with an OSB sheathing board and drywall was 3.25 W/m^{2}K (R-18.5). By including the thermal resistance of the drywall in an ICF wall assembly, the total resistance can be 4.01 m^{2}K/W (R-22.8). Therefore, the effective R-value of an ICF wall assembly is greater than that for a 2 in. × 6 in. wood stud frame construction with glass fiber. Note that for the ICF wall, the thermal resistance of the concrete is

Table 1. Dimension and thermal properties of the ICF components and glass fibre

Properties	Concrete	EPS[a]	Glass Fibre (Reference)
Thickness, δ, mm (inch)	152.4 (6 in.)	63.5 (2.5 in.)	140 (5.5 in.)
Thermal Conductivity, λ_{eff} (W/(m·K))	1.4	0.0332	0.039
Density, ρ (kg/m^3)	2,350	22.7	11.5
Specific Heat, Cp (J/(kg·K))	880	1,210 (ASHRAE 2009)	840
Volumetric Heat Capacity, ρCp (kJ/(m^3·K))	2,068	27.47	9.66
Thermal Diffusivity, $\alpha = \lambda_{eff}/(\rho Cp)$ (m^2/s)	6.77 x 10^{-7}	1.21 x 10^{-6}	4.04 x 10^{-6}
Characteristic Time Constant, $\tau = \delta^2/\alpha$ (hr)	9.53	0.93	1.35
Thermal Resistance, RSI = δ/λ_{eff} (m^2·K/W)	0.109	1.913	3.590
Total Thermal Resistance, R (ft^2 hr °F/Btu)	22.3[c]		20.4[b]

[a] Properties at 23°C
[b] Value does not include the effect of thermal bridging due to 2 in. × 6 in. studs
[c] Value does not include the effect of thermal bridging due to the plastic spanners

much lower than the EPS. As such, the main contribution of the concrete in the ICF walls to thermal performance is to provide thermal mass and ability to store thermal energy.

4. Characteristic time constant, τ, is another parameter that affects the transient response of a wall system. It is defined as $\tau = L_p^2/\alpha$, where L_p is the characteristic heat penetration length, which is equal to the thickness of material layer, δ. The characteristic time constant is a measure of the time that a material layer takes to complete 63.2% of the transient portion of its response due to a change in its thermal environment (63.2% response corresponds to 38.2% deviation from a steady-state condition, Rabin and Rittel 1999). As shown in Table 1, the characteristic time constant of a 6 in. thick concrete (9.53 h) is much larger than that for the 2.5 in. thick EPS (0.93 h). As such, the exterior and interior EPS layers respond quickly to the changes in the indoor and outdoor conditions. On the other hand, the concrete layer responds slowly to changes of thermal environment resulting in a small change in its temperature as will be shown later. For the glass fiber insulation, however, the characteristic time constant (1.35 h) is much smaller than that for concrete. Accordingly, the ICF wall responds slowly to the changes in thermal environment compared to the glass fiber wall.

In the next section, the governing equations and the initial and boundary conditions needed to predict the transient thermal response of wall systems are discussed.

GOVERNING EQUATIONS

The governing equations needed to assess only the thermal performance (no moisture transport) of wall systems are presented. The mass balance and momentum equations for airflow through porous medium are given as (Bird et al. 1960):

$$\text{Mass balance: } \varepsilon\frac{\partial \rho_f}{\partial t} = -\nabla \bullet \rho_f \vec{v}_f$$

$$\text{Darcy's Law: } \vec{v}_f = -\frac{k_f}{\mu_f}(\nabla P - \rho_f \vec{g}) \qquad (2)$$

where P is the air pressure, $\vec{g}$ is vector of acceleration due to gravity, $\vec{v}_f$ is Darcy velocity vector of the air, ρ_f is air density, ε is material porosity, k_f is air permeability, and μ_f is air dynamic viscosity.

The energy equation in porous media is given as (Saber et al. 2010a and 2010b):

$$\rho_o Cp_{eff}\frac{\partial T}{\partial t} + \rho_f Cp_f \vec{v}_f \bullet \nabla T = \nabla \bullet (\lambda_{eff}\nabla T) + q'''_{\text{source/sink}},$$

$$\text{with } \lambda_{eff} = \varepsilon\lambda_f + (1-\varepsilon)\lambda_s$$

$$\text{and } Cp_{eff} = Cp_s + \varepsilon Cp_f(\rho_f/\rho_o) \qquad (3)$$

where Cp_f and Cp_s are the specific heat of the fluid and solid, respectively, and λ_f and λ_s are the thermal conductivity of the fluid, and solid, respectively. The parameters ρ_o, λ_{eff} and Cp_{eff} in Equation 3 are the matrix density, apparent thermal conductivity and apparent specific heat, respectively, for a porous material. In Equation 3, the term $q'''_{\text{source/sink}}$ represents the heat source/sink (e.g., due to condensation/evaporation), which is neglected since no moisture transport was considered in this work. In this equation, the first term on the LHS represents the rate of accumulation in the thermal energy. The first term on the RHS accounts for heat transport by conduction and the second term on LHS accounts for heat transport by convection. In this study, it is assumed that there is no deficiency in the ICF wall specimen (e.g., no cracks). Furthermore, since both the air permeability of the EPS layers and the pressure difference across the wall are very small, the air leakage through the ICF wall specimen can be neglected. As such, the contribution in heat transfer by convection (second term

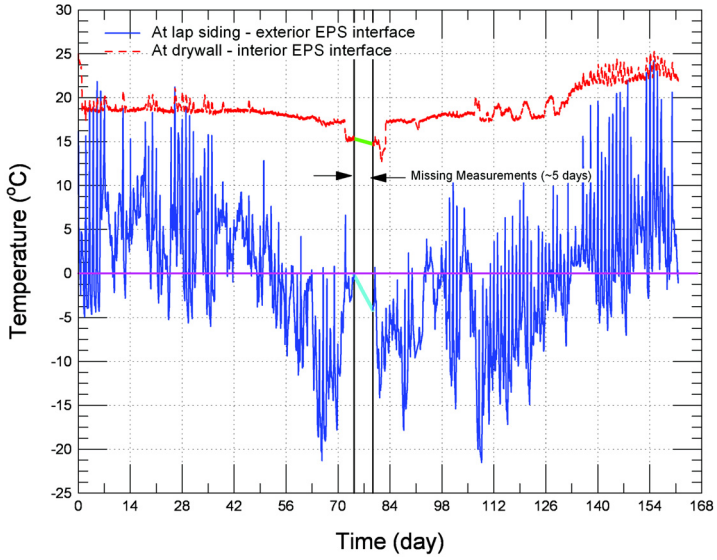

Figure 2 *Measured temperatures at vinyl siding—exterior EPS and drywall—interior EPS interfaces.*

on LHS of Equation 3) is zero; hence, there is no need to solve Equation 2.

Initial and Boundary Conditions

Figure 1 shows the mid-scale ICF wall specimens. Due to the symmetry, only one half of one ICF wall was modeled. The three-dimensional version of the present model was used in this study in order to account for the effect of thermal bridges due to wood frame around the ICF wall specimens. In a full-scale (2.4 m × 2.4 m) ICF wall system (no wood frame), however, the transient thermal response of this wall can be predicted using a one-dimensional thermal model. The initial temperature of the entire wall assembly was assumed uniform and equal to 10°C. Since this initial temperature is not the same as in the test, it is anticipated that the predicted dynamic response of the ICF wall in the first period of the test (say first 24–48 h) will be different than that obtained in the test.

The boundary conditions on the top, bottom, left, and right surfaces of the ICF wall are insulated and sealed (i.e., no heat transfer). In the test, the temperatures and heat fluxes were measured at different locations in the ICF wall specimens but were not measured on the exterior surface of the vinyl siding and on the indoor surface of the drywall. The temperature measurements were taken between the vinyl siding and the exterior EPS layer, on the face of the concrete behind the exterior EPS layer, on the face of the concrete behind the interior EPS layer, and between the drywall and the interior EPS layer. The measured temperatures at the vinyl siding—exterior EPS interface and at the drywall—interior EPS interface were taken as time-dependent boundary conditions for solving the energy equation (Equation 3). These measured temperatures are shown in Figure 2 where *Time* = 0 corresponds to October 13 at ~15:00. As shown in this figure, these measurements were missing during a period of five days (*Time* = 74.33 d–79.38 d). In numerical simulation, it was assumed that these temperatures changed linearly between *Time* = 74.33 d and *Time* = 79.38 d.

By considering the boundary conditions at vinyl siding—exterior EPS and drywall—interior EPS interfaces, there is no need to include both vinyl siding and drywall in the numerical simulations. In future work, however, numerical simulations will be conducted to investigate the transient response (including the effect of infiltration and exfiltration) of full-scale ICF wall assemblies subjected to different Canadian climates. The numerical simulation was conducted for a period of 161.66 d. The benchmarking of the present model against the experimental data and the transient response of the ICF wall are discussed next.

RESULTS AND DISCUSSION

Figure 3 shows the temperature contours in five vertical and horizontal slices passing through the ICF wall at the end of simulation (*Time* = 161.66 d). The first four vertical slices are passing through the ICF and the last vertical slice is passing through the wood frame on RHS of the ICF (Figure 3a). Figure 3 shows that the temperature distribution within the concrete layer is approximately uniform. Also, as shown in this figure, the wood frame in the mid-scale ICF assembly (see Figure 1) acts as thermal bridges due to its higher thermal conductivity (0.09 W/mK) compared to EPS (0.033 W/mK). A three-dimensional thermal model is needed to predict the thermal performance of wall systems with window and door

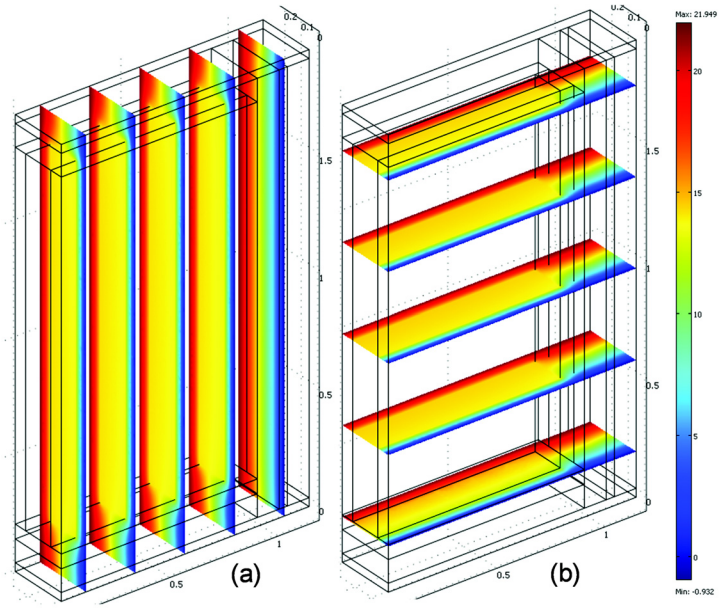

Figure 3 *Predicted temperature contours at the end of simulation (Time = 161.66 d).*

openings, corners, and structural joints with roofs, floors, ceilings, and other walls, where the effect of thermal bridges cannot be neglected. Simplifying the problem to one dimension can lead to errors in determining the energy efficiency of building envelope. However, for a clear/opaque ICF wall system (uninterrupted by wall details), the effect of these thermal bridges will be minimal, and the thermal performance can be accurately predicted by a one-dimensional thermal model.

During the first three months of the experiment, two heat flux transducers were positioned at the EPS-concrete interfaces. This proved a complex task due to the grooves in the interior side of the foam. To provide a flat surface for the heat flux transducers so that the measured heat flux component is perpendicular to the surface, a section of foam was removed prior to pouring the concrete. The grooves in the removed section of the EPS were filled in with wet concrete and cured before the foam section was put back into position (see Figure 4a). By doing this, the heat flux transducer was neither exposed to a uniform material nor in good contact with the material, but rather alternating lines of foam and concrete on the heat flux transducer surface (forming fins from both foam and concrete materials) with trapped air voids. The combined effect of both the fins (specifically the concrete ones since it has high thermal conductivity, 1.4 W/mK, compared to EPS, 0.033 W/mK, see Table 1) with the trapped air voids (thermal conductivity = 0.025 W/mK), called "fins effect" could result in different heat flux readings than the actual heat flux passing through the ICF assembly if the removed section of the foam shown in Figure 4a is in good contact with the surface of concrete.

When the measured heat fluxes were used to calculate the R-value of the ICF assembly during the periods of minimal change in the thermal environment (at pseudo steady-state conditions), it was found that the calculated R-value was R-14, which was much lower than the expected one (R~20). At this stage, it was decided to use the present model to interpret the results of the heat flux measurements and to improve the experiment design by repositioning the heat flux transducers at different locations in the EPS layers.

Figure 5 shows the predicted heat flux at different locations in the interior EPS layer at the wall center. As indicated earlier, *Time* = 0 corresponds to October 13th at ~15:00. As shown in this figure, the differences between the predicted heat fluxes at drywall—interior EPS interface, at the middle of the interior EPS, and at the interior EPS—concrete interfaces are small. The small differences between these heat fluxes are due to the small thermal mass of the EPS layer (see Table 1). Furthermore, when the predicted heat flux was used to calculate the R-value during the periods of pseudo steady-state conditions, the obtained R-value was approximately the same as expected for the ICF wall (R ~ 20).

During the first three months of the experiment (October 13 to January 14), the predicted heat flux at the middle of the interior EPS layer was compared with the measured heat flux at the interior EPS—concrete interface at the center of wall in Figure 6. As shown in this figure, the trends of both the measured and predicted heat fluxes with time are approximately the same.

Figure 4 *Installation of heat flux transducer in the ICF test specimen.*

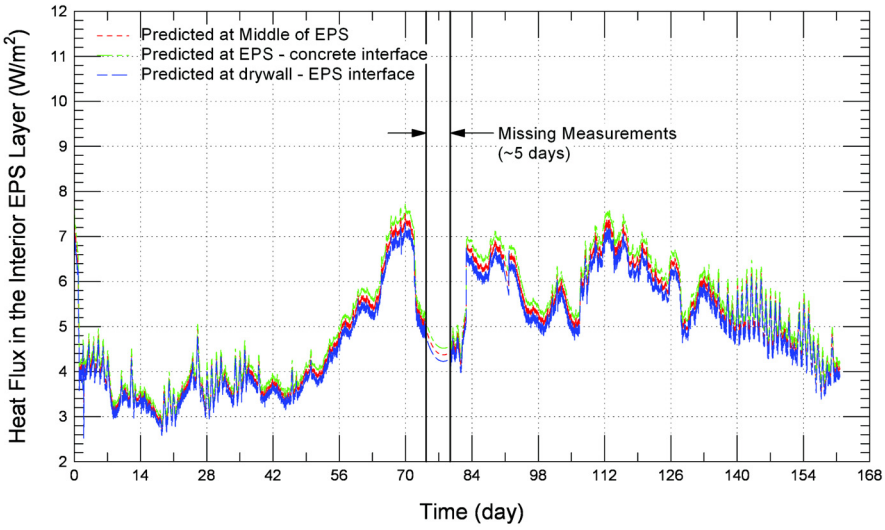

Figure 5 *Predicted heat flux at different locations in the interior EPS layer at the center of the wall.*

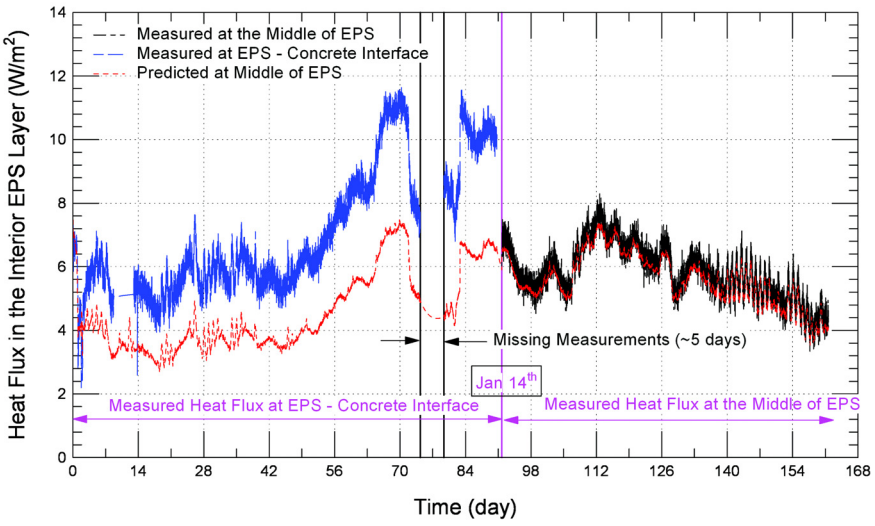

Figure 6 *Comparison of predicted and measured heat fluxes in the interior EPS layer at the center of the wall.*

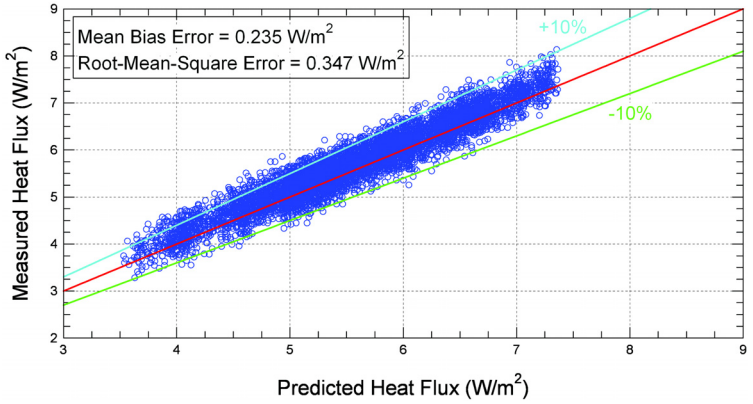

Figure 7 *Comparison between the measured and predicted heat fluxes at the middle of the interior EPS after repositioning the heat flux transducer (January 14).*

However, the measured heat flux was ~30% higher than the predicted one due to the fin effect as indicated earlier. Consequently, it was decided to expose the heat flux transducers that were installed at the exterior EPS—concrete interface and at the interior EPS—concrete interface to a uniform material by repositioning them between two blocks of foam (approximately at the middle of the EPS layers as shown in Figure 4b). By doing this, it was possible to expose the heat flux transducers to uniform material and to ensure that these heat flux transducers were in a good contact with the EPS material and with homogenous material. Full descriptions of the instrumentation of the experiment and test results will be reported at a later date. Thereafter, the predicted results using the present model were compared with the measurements. During the last period of the experiment (January 14 to March 24, after repositioning the heat flux transducers), Figure 6 shows a comparison between the predicted and measured heat fluxes at the middle of the interior EPS layer. During this period, a quantitative statistical measure of the agreement between the predicted and measured heat fluxes at the middle of the interior EPS layer is also shown in Figure 7. As shown in Figure 6 and Figure 7, the agreement between the model prediction and experiment is reasonably good (within ~+10%). Furthermore, the mean bias error and root-mean-square error between the model prediction and experiment were 0.235 W/m^2 and 0.347 W/m^2, respectively.

In the exterior EPS layer, Figure 8 shows a comparison between the predicted heat fluxes at the concrete—EPS interface, at the middle of the EPS and at the EPS—vinyl siding interface at the center of wall. As shown in this figure, the differences between the predicted heat fluxes at different locations are very small. Given that the EPS has a small thermal mass (see Table 1) and the temperature at vinyl siding—EPS interface changes significantly with time (see Figure 2), the exterior EPS layer has a fast thermal response. As such, the predicted heat fluxes in the exterior EPS layer change significantly with time (Figure 8).

During the first period of the experiment from October 13 (day 0) to January 29 (day 108), the predicted heat flux at the middle of the exterior EPS layer is compared with measured one at the concrete – EPS interface in Figure 9 at the center of wall. Similar to the case of interior EPS layer, the measured heat flux was ~30% higher than the predicted one (e.g., see Figure 10 for a period of two weeks from day 56 to day 70). On January 29 (day 108), the heat flux transducer at the concrete—exterior EPS interface was repositioned at the middle of the exterior EPS (Figure 4b). During the last period of the test (January 29 to March 24), Figure 9 shows a comparison between the measured heat flux at the middle of exterior

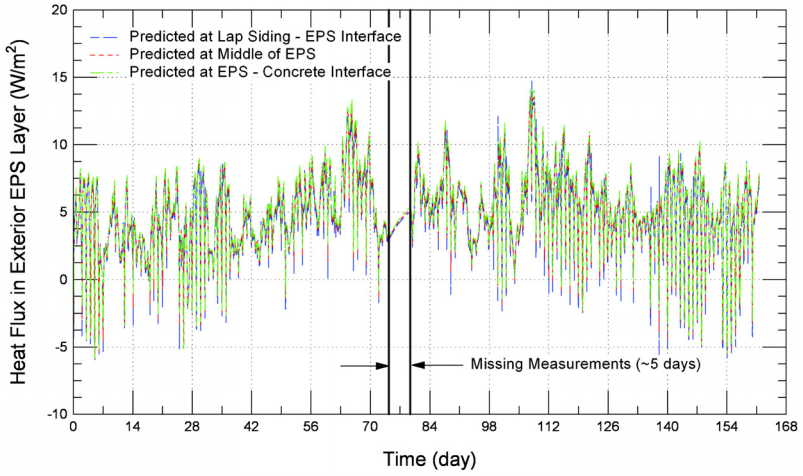

Figure 8 *Predicted heat flux at different locations in the exterior EPS layer at the center of wall.*

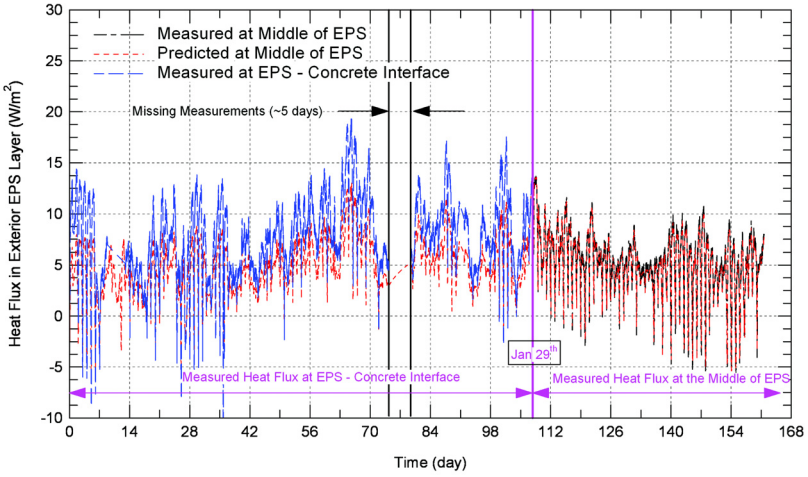

Figure 9 *Comparison of predicted and measured heat fluxes in the exterior EPS layer at the center of the wall.*

EPS with the predicted one. During this period, Figure 11 shows a quantitative statistical measure of the agreement between the predicted and measured heat fluxes at the middle of the exterior EPS layer. The mean bias error and root-mean-square error between the model prediction and experiment were 0.126 W/m^2 and 0.630 W/m^2, respectively. Figure 9 and Figure 11 show the agreement between the model prediction and experiment is reasonably good (within ~+10%).

A final step for benchmarking the present model was conducted by comparing its prediction for the heat flux at the vinyl siding—exterior EPS interface with the measured one at the center of wall. This comparison is shown in Figure 12. Despite the large scatter in measured heat flux at the vinyl siding—EPS interface during the last period of the test, Figure 12 shows that both predicted and measured heat fluxes are in good agreement.

SUMMARY AND CONCLUSION

This paper is one of a series to benchmark the NRC-IRC's hygrothermal model, called hygIRC-C. This model solves simultaneously the two-dimensional and three-dimensional Heat, Air, and Moisture (HAM) transport equations. However, no moisture transport was considered in this study. During the first period of the test, the readings of the heat flux transducers

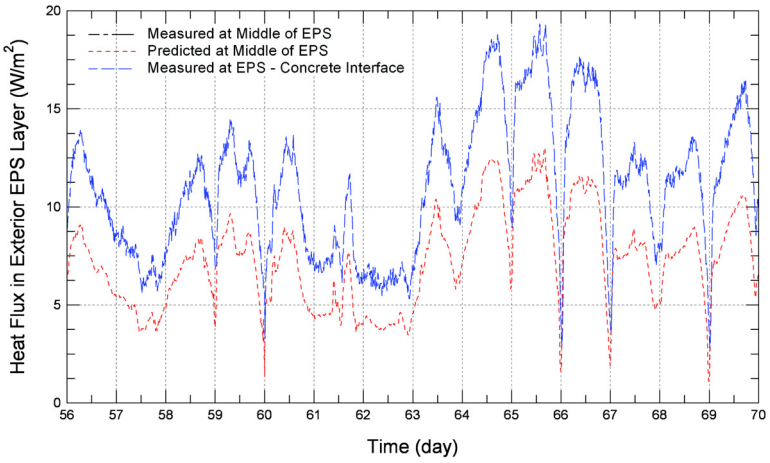

Figure 10 *Enlargement of Figure 9 for a period of 2 weeks (time = 56 d – time = 70 d).*

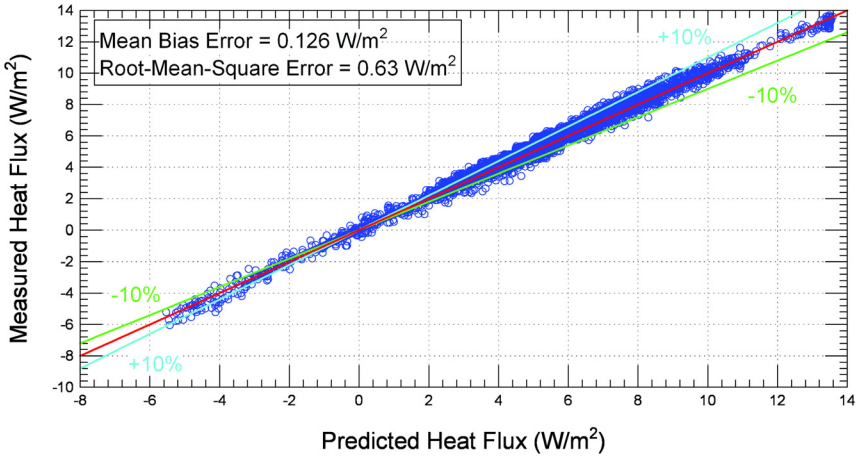

Figure 11 *Comparison between the measured and predicted heat fluxes at the middle of the exterior EPS after repositioning the heat flux transducer (January 29).*

that were positioned at the EPS-concrete interfaces were used to determine the R-value of the ICF test specimens. It was found that the calculated R-value during the periods of pseudo steady-state conditions (i.e., during the periods of minimal change in the thermal environment) was much lower than the expected R-value. The present model was then used to interpret the results of the heat flux measurements and to improve the experiment design by repositioning the heat flux transducers at different locations in the EPS layers. As a result of the small thermal mass of the EPS, the numerical results showed that the differences between predicted heat fluxes at different locations in each EPS layer were small. As such, it was decided to reposition these heat flux transducers at the middle of the EPS layers. Thereafter, the numerical results were compared with the measurements. The results showed that the comparison between the present model predictions and experimental data was reasonably good (within ~+10%). This research is on-going. The present model will be used to conduct numerical simulations in order to investigate the transient thermal response of full-scale ICF wall assemblies subjected to different Canadian climate conditions. The results of this effort will be the subject for future publications.

ACKNOWLEDGMENTS

The authors wish to thank Anil Parekh at Natural Resources Canada (NRCan) and Silvio Plescia at Canada Mortgage and Housing Corporation (CMHC) for providing guidance and contributing funding for this project. Funding from NRC has enabled NRC-IRC to build, operate, and maintain a state-of-the-art Field Exposure of Walls facility (FWEF). Our thanks are also extended to Ross Monsour at Ready Mix Concrete Association of Ontario (RMCAO) for his contribution in providing the test specimens and NRC-IRC colleague Mike Nicholls for his precious technical contribution.

REFERENCES

ASHRAE. 2009. 2009 ASHRAE Handbook—Fundamentals (SI). 26.5. Atlanta: American Society of Heating, Refrigerating, and Air-Conditioning Engineers Inc.

ASTM Designation: C 518-04, Steady-State Thermal Transmission Properties by Means of the Heat Flow Meter Apparatus, Section 4, Volume 04.06, Thermal Insulation, 2007 Book of ASTM Standards.

ASTM Designation: C 1130-07, "Standard Practice for Calibrating Thin Heat Flux Transducers", Annual Book of ASTM Standards, sec 4, Construction, vol 04.06, Thermal Insulation; Building & Environment Acoustic, pp. 577–84, 2009.

Bird, R.B., W.E. Stewart, and E.N. Lightfoot. 1960. Transport Phenomena, John Wiley & Sons, Inc., pp. 149-150.

Burch, D.M., W.L. Johns, T. Jacobsen, G.N. Walton, and C.P. Reeve. 1984a. "The Effect of Thermal Mass on Night Temperature Setback Savings." ASHRAE Transactions, 90(part 2), 184–206.

Burch, D.M., K.L. Davis, and S.A. Malcomb. 1984b. "The Effect of Wall Mass on the Summer Space Cooling of Six Test Buildings." ASHRAE Transactions 90 (part 2), 5–21.

Burch, D.M., D.F. Krintz, and R.F. Spain. 1984c. "The Effect of Wall Mass on Winter Heating Loads and Indoor Comfort—An Experimental Study." ASHRAE Transactions 90 (part 1), 94–114.

Christian, J.E. 1991. "Thermal Mass Credits Relating to Building Energy Standards." ASHRAE Transactions 97 (part 2), 941-957.

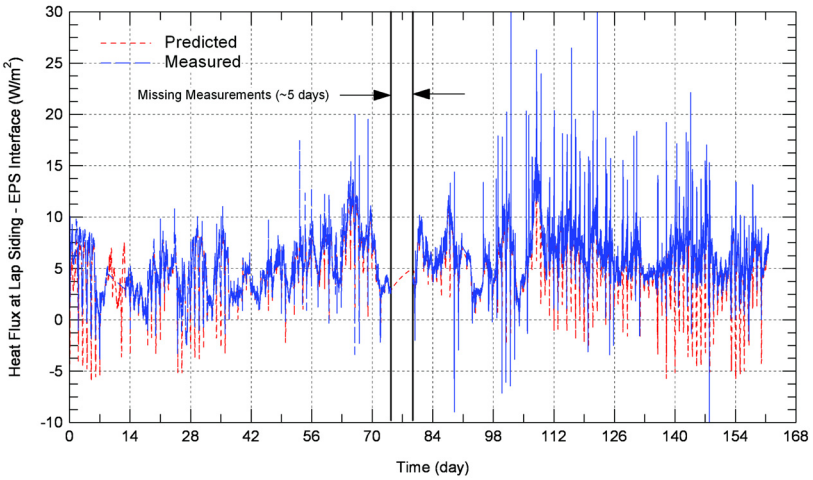

Figure 12 *Comparison of predicted and measured heat fluxes at vinyl siding—EPS interface at the center of wall.*

Christian, J.E., J. Kosny, A.O. Desjarlais, and P.W. Childs. 1998. “The Whole Wall Thermal Performance Calculator–On the Net.” In Proceedings, Thermal Performance of the Exterior Envelopes of Buildings VII, 287–99. Atlanta, Ga.: American Society of Heating, Refrigerating and Air-Conditioning Engineers.

COMSOL Multiphysics, version 3.5a, www.comsol.com.

Elmahdy, A.H., W. Maref, M.C. Swinton, H.H. Saber, and R. Glazer. 2009. Development of energy ratings for insulated wall assemblies. Building Envelope Symposium, San Diego, California, October 26, 2009, pp. 21–30.

Gajda, J., 2001. Energy Use of Single-Family Houses with Various Exterior Walls. Research & Development Information Report. Portland Cement Association and Concrete Foundations Association. PCA CD026. PP 1-46.

Hersh Servo AG. 2010. Insulated Concrete Forms [online]. Available from: http://www.hirsch-gruppe.com [accessed 29 April 2010].

Hill, D., and R. Monsour. Monitored Performance of an Insulating Concrete Form Multi-Unit Residential Building, Draft Final Report, prepared by Enermodal Engineering Limited, www.enermodal.com, September 2006.

Kosny, J., E. Kossecka, A.O. Desjarlais, and J.E. Christian. 1998. “Dynamic Thermal Performance of Concrete and Masonry Walls.” In Proceedings, Thermal Performance of the Exterior Envelopes of Buildings VII, 629-643. Atlanta, Ga.: American Society of Heating, Refrigerating and Air-Conditioning Engineers.

Kosny, J., T. Petrie, D. Gawin, P. Childs, A. Desjarlais, and J. Christian. 2001. “Energy Benefits of Application of Massive Walls in Residential Buildings.” In Proceedings, Performance of Exterior Envelopes of Whole Buildings VIII, Session IX-A. Atlanta, Ga.: American Society of Heating, Refrigerating and Air-Conditioning Engineers.

Kossecka, E., and J. Kosny. 1998. “Effect of Insulation and Mass Distribution in Exterior Walls on Dynamic Thermal Performance of Whole Buildings.” In Proceedings Thermal Performance of the Exterior Envelopes of Buildings VII, 721-731. Atlanta, Ga.: American Society of Heating, Refrigerating and Air-Conditioning Engineers.

Maref, W., M.K. Kumaran, M.A. Lacasse, M.C. Swinton, and D. van Reenen. “Laboratory measurements and benchmarking of an advanced hygrothermal model”, Proceedings of the 12th International Heat Transfer Conference, Grenoble, France, August 18, 2002, pp. 117-122 (NRCC-43054).

NAHB Research Center. 1999. “Insulating Concrete Forms: Comparative Thermal Performance” prepared for U.S. Dept. of Housing and Urban Development. August 1999.

Petrie, T., J. Kosny, A. Desjarlais, J. Atchley, P.W. Childs, M.P. Ternes, and J. Christian. 2001, “How Insulating Concrete Form vs. Conventional Construction of Exterior Walls Affects Whole Building Energy Consumption: Results from a Field Study and Simulation of Side-by-Side Houses”

Rabin, Y., and D. Rittel. “A Model for the Time Response of Solid-embedded Thermocouples”, Experimental Mechanics, VoL 39, No. 2, pp. 132-136, 1999.

Saber, H.H., W. Maref, A.H. Elmahdy, M.C. Swinton, and R. Glazer. “Three-Dimensional Thermal Model for Predicting the Thermal Resistances of Spray Polyurethane Foam Wall Assemblies”, Building XI conference, Clearwater, Florida, 2010a.

Saber, H.H., W. Maref, M.A. Lacasse, M.C. Swinton, and K. Kumaran. “Benchmarking of Hygrothermal Model against Measurements of Drying of Full-Scale Wall Assemblies” International Conference on Building Envelope Systems and Technologies, ICBEST 2010, Vancouver, Canada, June 27-30, 2010b.

Saber, H.H., and M.C. Swinton. “Determining through Numerical Modeling the Effective Thermal Resistance of a Foundation Wall System with Low Emissivity Material and Furred – Airspace” International Conference on Building Envelope Systems and Technologies, ICBEST 2010, Vancouver, Canada, June 27-30, 2010.